OPEN

NPG Asia Materials (2016) 8, e234; doi:10.1038/am.2015.138
www.nature.com/am

ORIGINAL ARTICLE

Coordination of the electrical and optical signals revealing nanochannels with an 'onion-like' gating mechanism and its sensing application

Xuemei Xu[1], Wei Zhao[2], Pengcheng Gao[1], Huiqing Li[3], Guang Feng[2], Zujin Zhao[4] and Xiaoding Lou[1]

Artificial stimuli-responsive nanochannels that mimic the gating property of biological ion channels to control the movement of ions across the membranes have attracted much attention. However, the ionic current is also greatly influenced by many environmental factors in the reaction system. In the present study, we coordinated the ionic current and the fluorescence signal to reveal that the gatekeepers (here, oligomers) open and close the nanochannels with an 'onion-like' intermediate state, as confirmed by molecular dynamics simulations. The dual-signal-output nanochannels exhibited a high sensitivity and selectivity to glucose and showed a high antijamming property with regard to impurities such as ascorbic acid (Vc) and H_2O_2 in complicated practical environments, which could induce false signals in traditional glucose detection methods. Ten healthy individuals' urine samples were distinguished from those of 15 diabetes patients; moreover, the urine samples of the diabetes patients could be discriminated before and after treatment with insulin.

NPG Asia Materials (2016) **8,** e234; doi:10.1038/am.2015.138; published online 8 January 2016

INTRODUCTION

Ion channels, which are embedded within cell membranes, are used by the cell to chemically and electrically communicate with the extracellular world and are the basis of many cellular functions, including brain activity, insulin secretion[1] and ion transport across membranes.[2] Most ion channels are not permanently open; rather, they can be selectively opened and closed in response to extracellular signals, allowing the cell to control the movements of ions across the membrane, thus serving as 'smart' gates that regulate the internal environment. In recent years, researchers have made efforts to develop bioinspired smart nanochannels that mimic the function of gating property of biological ion channels for use in various applications, such as biosensors,[3–10] nanofluidic devices[11–14] and molecular filtration.[15,16] Monitoring the ionic current across a nanochannel is the conventional investigation method used to decode the properties of research subjects, such as size, structure, conformation and dynamic motion.

The highly useful capability of electrical approaches is solely the investigation of the ionic current flowing through nanochannels; however, the ionic current is greatly influenced by many environmental factors in the reaction system. Among these, two types of influence factors should be considered: (i) non-specific adsorption to the surface of solid-state nanochannels, which would affect the ion pathways and may cause false signals during the gating process,[17,18] and (ii) the ionic current on the edge (such as the part embedded within cell membranes) behaves differently than the inner part of ion channels. For example, it is possible to observe a current blockade even if the molecules are at the channel tip rather than in the channel lumen.[19,20]

In addition, the ionic current provides temporal information instead of spatial information on the process of gating, which makes it difficult to investigate the mechanism of gating. To address these limitations, the incorporation of additional measurements that supplement the electrical measurements to validate the envisaged gating process through the ion channels is indispensable.[21,22] Among many techniques, fluorescent imaging is well established in studying the behavior of molecules in a variety of confined spaces.[23] By combining ionic current signal with molecule fluorescence imaging, we will directly observe whether the decrease in ionic current does in fact correspond to the blockade of the channels by ambient stimuli.

Recently, translocation of the targets through a pore has been combined with microscope-based fluorescence imaging and electrical signal.[24–30] One exciting work reported by Heron *et al.*[24] shows that the ionic current and fluorescence from single protein pores can simultaneously be detected and that the electrical events can be unambiguously assigned to specific channels. The availability of two independent signals reveals additional analytic capabilities but also

[1]Hubei Key Laboratory of Bioinorganic Chemistry & Materia Medica, Key Laboratory for Large-Format Battery Materials and System, School of Chemistry and Chemical Engineering, Huazhong University of Science and Technology, Ministry of Education, Wuhan, PRC; [2]State Key Laboratory of Coal Combustion, Huazhong University of Science and Technology, Wuhan, PRC; [3]Department of Endocrinology, Union Hospital, Tongji Medical College, Huazhong University of Science and Technology, Wuhan, PRC and [4]State Key Laboratory of Luminescent Materials and Devices, South China University of Technology, Guangzhou, PRC
Correspondence: Professor X Lou, Hubei Key Laboratory of Bioinorganic Chemistry & Materia Medica, Key Laboratory for Large-Format Battery Materials and System, School of Chemistry and Chemical Engineering, Huazhong University of Science and Technology, Wuhan 430074, PRC.
E-mail: louxiaoding@hust.edu.cn
Received 1 September 2015; revised 14 October 2015; accepted 20 October 2015

raises challenges for more complex solutions including multiple targets. However, the dual-signal-output nanochannel integration of the oligomerization reaction, fluorescence and electrical control in solid-state nanochannels has not been demonstrated.

Here, we present a solid-state nanochannel system incorporated as a 'smart gate' that not only ensures the controlled delivery of targets for electrical detection, but also provides a characteristic fluorescent signal for additional analysis. The dual-signal-output nanochannel system is a new platform for studying the gating process that is more powerful than either method alone. To observe the fluorescent signal, we are interested in a group of fluorogens that are non-emissive when molecularly dissolved, but highly luminescent when supramolecularly aggregated. This phenomenon is called aggregation-induced emission (AIE); the restriction of intramolecular motions (RIM) is proposed as the mechanism.[31–33] One can observe the AIE phenomenon in the molecules containing rotating units, such as phenyl rings. In dilute solutions, the rotor-containing fluorogens are non-emissive because of the low-frequency motions that cause the rapid nonradiative decay of the excited states (fluorescence off). By contrast, in the aggregation state, these motions are blocked by the RIM, which opens up the radiative pathway (fluorescence on). In this study, functional-group-modified fluorogen ((1,2-diphenylethene-1,2-diyl) bis (1,4-phenylene)-1,1′-diboronic acid (TPEDB)) was selected to interact specifically with glucose (Glu), leading to the formation of oligomers.[31] It can be speculated that if oligomers formed, nanochannels would generate effective blockade of transmembrane ionic current (open-to-close) as well as the emission of the fluorescence signal (off-to-on) owing to the folding and aggregation of oligomers, acting as dual-signal-output (electric and fluorescence) system. More importantly, with the aid of the simultaneous monitoring of the fluorescence signals and analysis of the transmembrane ionic current, we successfully developed a theoretical model of the ion-channel gating via a dynamics study.

EXPERIMENTAL PROCEDURES

Polyethylene terephthalate membranes (PET, ~12 μm thick) were irradiated with Au ion beam (11.4 Mev per nucleon in GSI, Darmstadt, Germany). The track density is $\sim 5 \times 10^7$ cm^{-2}. Before etching the ion tracks, the membranes were irradiated with UV light for 1 h on each side. Next, the PET membranes were chemically etched in 2 M NaOH solution at 50 °C for 5 min to obtain cylindrical nanochannels. After etching, the PET membranes were thoroughly washed with and then restored in distilled water for at least 5 h to remove the inside residual etchant. The morphology of the nanochannels surface was imaged using field-emission scanning electron microscopy (Sirion SEM 200, FEI, Eindhoven, The Netherlands). The statistical results show that the diameter of the nanochannels is ~27 ± 3 nm (Supplementary Figure S1).

As a result of chemical etching, carboxyl groups were generated on the interior wall surface of the nanochannels. To immobilize the 4-aminophenylboronic acid (capture probe) in the nanochannels, track-etched PET membranes were immersed in 600 μl solution containing 6 mg of NHSS and 30 mg of EDC•HCl for 10 h at 4 °C. During this process, NHSS esters were formed. Next, the PET-NHSS ester monolayers were reacted with a solution containing 1 mM 4-aminophenylboronic acid for 10 h, resulting in the formation of covalent bonds. Finally, the film was washed three times with distilled water.

The transmembrane ionic current was recorded with a Keithley 6487 picoammeter (Keithley Instruments, Inc., Cleveland, OH, USA). A pair of Ag/AgCl electrodes was used to measure the resulting ionic current. The membrane was mounted between two halves of the conductance cell. Both halves of the cell were filled with a 50 mM phosphate-buffered solution (pH = 7.48). A scanning triangular voltage signal running from −0.2 to 0.2 V with a period of 40 s was selected.

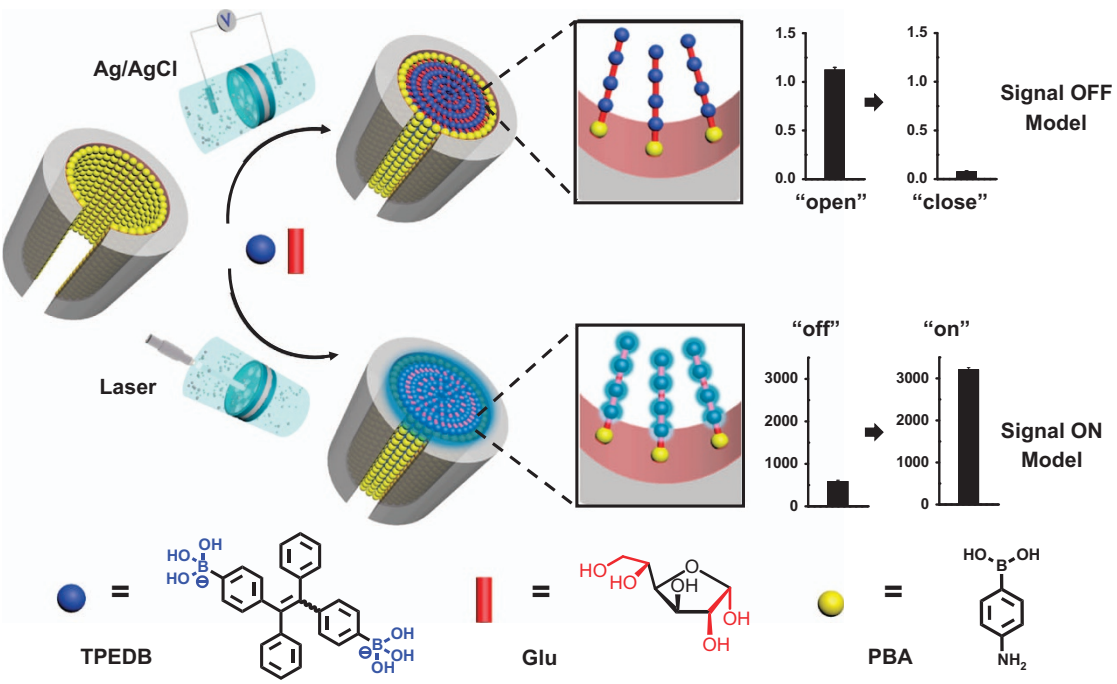

Figure 1 Schematic of the ionic current and fluorescent dual-signal-output nanochannels in the oligomerization process. The nanochannels are first modified with capture probes (4-aminophenylboronic acid (PBA)). In the presence of aggregation-induced emission (AIE) molecules ((1,2-diphenylethene-1,2-diyl) bis (1,4-phenylene)-1,1′-diboronic acid (TPEDB)), an oligomerization reaction between TPEDB and diol-contained glucose (Glu) occurs on the capture probe of the channel wall. With the reversible boronic acid-diol interaction occuring in nanochannels, the pathway for ion transport is blocked (upper panel), resulting in the sharp decrease of the ionic current (the close state). At the same time, when the TPEDB is oligomerized with glucose, the restriction of the intramolecular motion (RIM) process to fluorogen is activated (bottom panel); as a result, the emission is greatly boosted (fluorescence turned on).

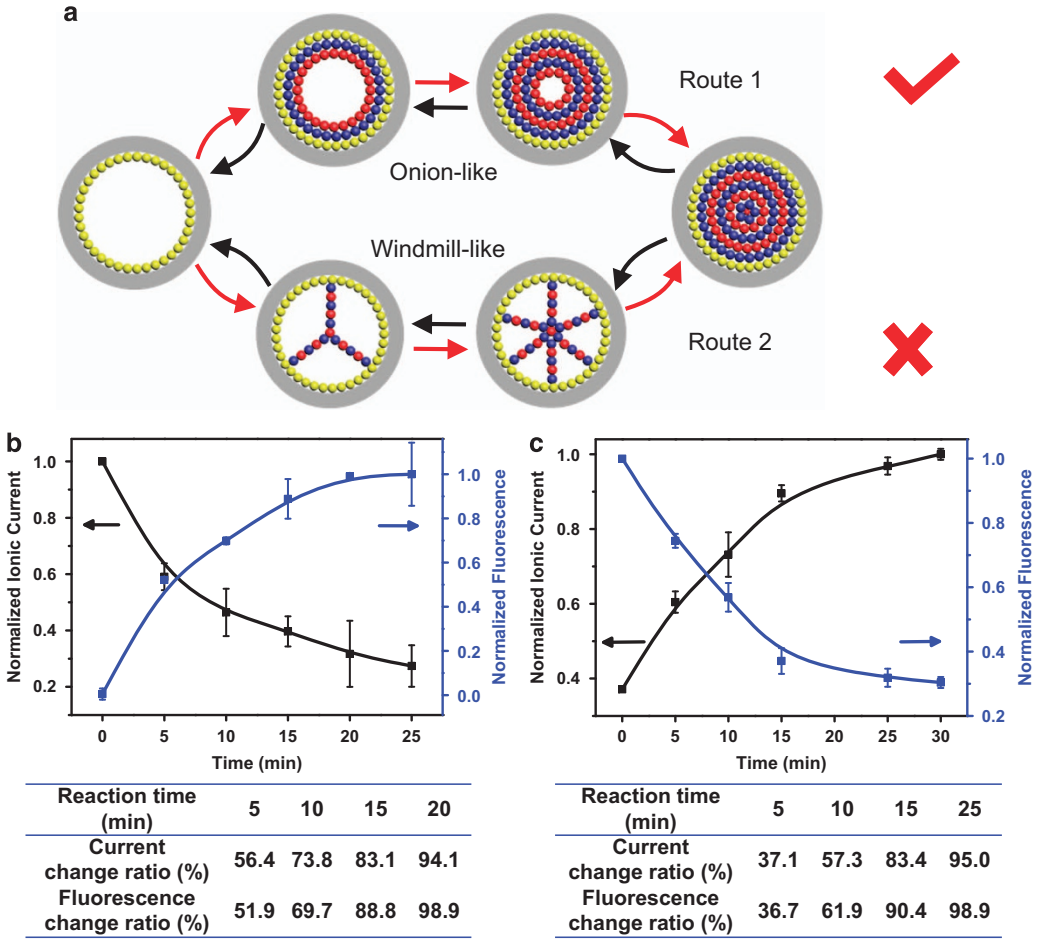

Reaction time (min)	5	10	15	20
Current change ratio (%)	56.4	73.8	83.1	94.1
Fluorescence change ratio (%)	51.9	69.7	88.8	98.9

Reaction time (min)	5	10	15	25
Current change ratio (%)	37.1	57.3	83.4	95.0
Fluorescence change ratio (%)	36.7	61.9	90.4	98.9

Figure 2 Mechanistic study of the blockage and opening of nanochannels. (**a**) Two conceivable routes are proposed: an 'onion-like' model (route 1) and a 'windmill-like' model (route 2). (**b**) The oligomer formation process (open-to-close) monitored by real-time current and fluorescence. (**c**) The dissociation process of oligomers (close-to-open) monitored by our dual-signal-output nanochannels at different times.

Confocal images were acquired using an Olympus biological confocal laser scanning unit mounted on a FV1200 microscope (Olympus Corporation, Tokyo, Japan; excitation: 405 nm; emission collected: 425–525 nm).

RESULTS AND DISCUSSION

Initially, cylindrical nanochannels in the PET membrane are prepared according previously described processes (Supplementary Figure S1).[34–36] Next, capture probes (4-aminophenylboronic acid (PBA)) are immobilized onto the nanochannel walls via a two-step chemical reaction (Supplementary Figure S2A). After the addition of TPEDB and Glu in the environmental solution, diboronic acids reversibly form stable boronate complexes with cis-diols, resulting in the formation of the oligomers $(TPEDB\text{-}Glu)_n$ on the channel walls (Supplementary Figure S2B). The general design of the ionic current/fluorescence dual-signal-output nanochannels is shown in Figure 1, where an oligomerization reaction between diboronic acid-based fluorophore (TPEDB) and diol-contained Glu is displayed on phenylboronic acid that is attached to the channel wall and serves as a capture probe. With the formation of the reversible boronic acid-diol interaction in the nanochannels, the pathway for ion transport is blocked. As a result, the ionic current sharply decreases. In addition, TPEDB is a propeller-shaped molecule that is weakly fluorescent in alkaline solution (carbonate buffer containing 2 vol% DMSO, pH = 10.5). The emission is greatly boosted when the TPEDB is oligomerized with Glu owing to the RIM process.[31] Applying these findings, we can obtain both electric and fluorescence signals from this oligomerization process.

The ionic current across the channels is measured to monitor the oligomerization reaction process and the gating performance of these PBA-modified nanochannels. After modification with the capture probe (PBA), only very limited reduction in the transmembrane ionic current is found (Supplementary Figures S3 and S4). By contrast, when oligomers $(TPEDB\text{-}Glu)_n$ are formed, the transmembrane ionic current sharply decreases from 1.09×10^{-6} A (the open state) to 6.65×10^{-8} A (the closed state), with an ON–OFF ratio of 16.5 (Figure 1, top right). The successful oligomerization of TPEDB and Glu in the nanochannels is verified by laser scanning confocal microscopy (Figure 1, bottom right). Without Glu, PBA-modified nanochannels are non-emissive in a carbonate buffer (turned off). The PBA-modified nanochannels emit light upon the addition of Glu, with an intensity of 5.5-fold higher than that in the absence of Glu (turned on).

The data presented above prove that the formation of oligomers $(TPEDB\text{-}Glu)_n$ on the channel wall induce both the current blockade and the enhancement of the fluorescence. However, instead of taking a single path, the oligomerization reaction inside the nanochannels likely occurs via one of two different routes, as shown in Figure 2a. Thus, the following experiments are conducted to explore the above two possible

routes and determine the most efficient one. To determine the oligomerization process in nanochannels, a quantitative analysis of the current and fluorescence changes during this process is performed (Figure 2b). The time curve of the oligomers formation shows that the transmembrane ionic current decreases rapidly with reaction time. The ratios of the current changes (I_0–I/I_{max}–I_{min}) at 5, 10, 15 and 20 min are 56.4, 73.8, 83.1 and 94.1%, respectively, and the corresponding ratios of fluorescence changes (F–F_0/F_{max}–F_{min}) are 51.9, 69.7, 88.8 and 98.9%, respectively (inset table of Figure 2b). The above data show that the changes in the two signals (ionic current and fluorescence) keep pace with each other, which proves that oligomers are formed via route 1 (red arrow), namely, an 'onion-like' intermediate state. Otherwise, the fluorescence change would be faster than the ionic current change owing to the current-voltage properties of nanochannels and the fluorescent properties of TPEDB.[36] It is known that the affinity of boronic acids to diols at low pH is small. Therefore, the Glu responsiveness can be adjusted by pH. In the following study, Glu molecules are released from the oligomers by immersing the membrane in a pH 2 solution. The dissociation of phenylboronic acid cyclic ester leads to the increment of transmembrane ionic current and reduction of fluorescence intensity with a similar time course; that is, hydrolysis of the oligomers occurred via route 1 (onion-like, black arrow).

To verify the fundamental formation and dissociation mechanism of the oligomers, we used a molecular dynamic (MD) system, shown in Figure 3, in order to identify the preferred intermediate state at the molecular level.[37] The oligomers were modeled by a coarse-grained model of a polymer (decane). The nanochannels were modeled by two concentric layers of carbon substrate with an inner layer diameter of 20 nm and a gap of 0.5 nm between the layers. The substrate was modeled by carbon atoms with a distance of 0.3 nm between each of the two neighbors, and the growing point (capture probe) on the inner layer was modeled by a silica atom, which has a stronger interaction with the polymer than carbon substrate. Different nanochannel-filling fractions (f = 25, 50, 75 and 100%) were determined by the number of polymers with respect to that in the full-loading case (Supplementary Figures S5). More simulation details can be found in the Supplementary Information. As seen in Figure 3, the polymers grow according to the onion-like model. Because the oligomerization process is dynamic, the movements of the polymers in the nanochannels are also simulated by the MD system. The movements of the polymers are random at the beginning (even if they are initially set at a 'windmill-like' state), but the movements finally result in an onion-like state (Supplementary Video 1: 50% filling; Supplementary Video 2: 75% filling). Thus, the practicability of an onion-like intermediate state was predicted by MD simulation, which solidly supports the mechanism of the oligomer formation process presented in Figure 2.

Under the optimized conditions, the modified PET membrane is immersed in a solution containing TPEDB and Glu at a predetermined concentration for 20 min before electrical measurements are performed. The current-voltage (I-V) curves show that the PBA-modified nanochannels displayed a Glu response with a high sensitivity (Figure 4a and Supplementary Figure S9). Upon the addition of 0.4 μM of Glu, a decrease of over 40% in the conductance of the nanochannels is observed. Increasing the target to 4 mM, the ionic conductance decreases by >90% of the initial value (Figure 4b). These results are relatively better, ensuring a detection range of 0.1–0.8 mM, which is the urine Glu level (urine sugar contains mainly Glu) in Glu-negative urine specimens.[38] At the same time, the fluorescence intensity increased with increments in the amount of Glu (Figure 4c). When the concentration of Glu is 4 μM, the nanochannels become very emissive, with an intensity of 5.5-fold higher than that in the absence of Glu (Figure 4d).

For selective sensing of saccharides, a great challenge is the binding selectivity because many saccharides (especially monosaccharides) show no difference between the structural group and the functional group (hydroxyl group), except in the configurations of certain stereocenters, thus making recognition extremely difficult.[39] In this work, Glu and five other simple D-sugars (xylose, arabinose, mannose, fructose and galactose) are used to investigate the effects of transmembrane ionic current changes of the nanochannels on the interactions with different sugars (Supplementary Figure S10). As shown in Figure 5a, the detection of Glu formed between bifunctional TPEDB and divalent Glu is highly selective because of the existence of a pair of *cis*-diol units in the 1,2- and 5,6-positions. By contrast, once reacted with a boronic acid unit, other saccharides have no additional diol unit with a *cis*-conformation to further react with TPEDB to form oligomeric species.[40] As a result, high selectivity was observed during this oligomerization reaction in PBA-modified nanochannels.

To examine whether the oligomerization reaction indeed has an essential role in this dual-signal-output process, we prepared a monosubstituted TPE derivative (4-(1,2,2-triphenylvinyl)phenylboronic acid (TPEB), Supplementary Figure S11) with one boronic acid unit, which is incapable of undergoing the oligomerization reaction. Expectedly, neither the ionic current nor the fluorescence signal exhibits an

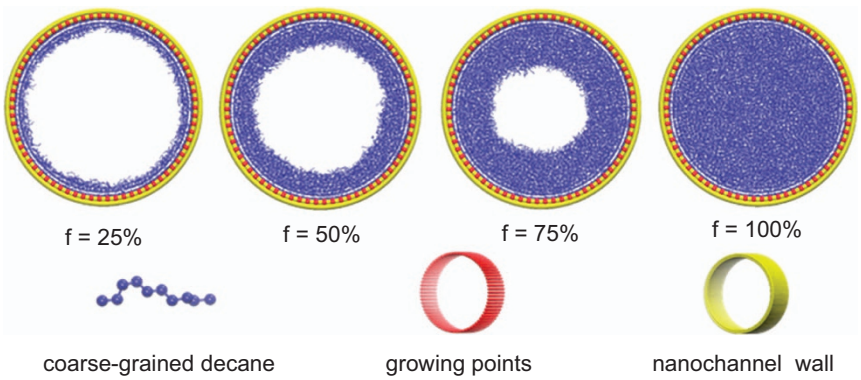

Figure 3 Snapshot of the molecular dynamics (MD) system that is fully/partially filled with coarse-grained polymers (decane). The substrate is modeled by carbon atoms with a distance of 0.3 nm between each of the two neighbors, and the growing point (capture probe) on the inner layer is modeled by a silica atom, which has a stronger interaction with polymer than carbon substrate. This MD simulation solidly supports the mechanism of the 'onion-like' intermediate state of oligomer formation process. *f* indicates the filling fraction of polymers.

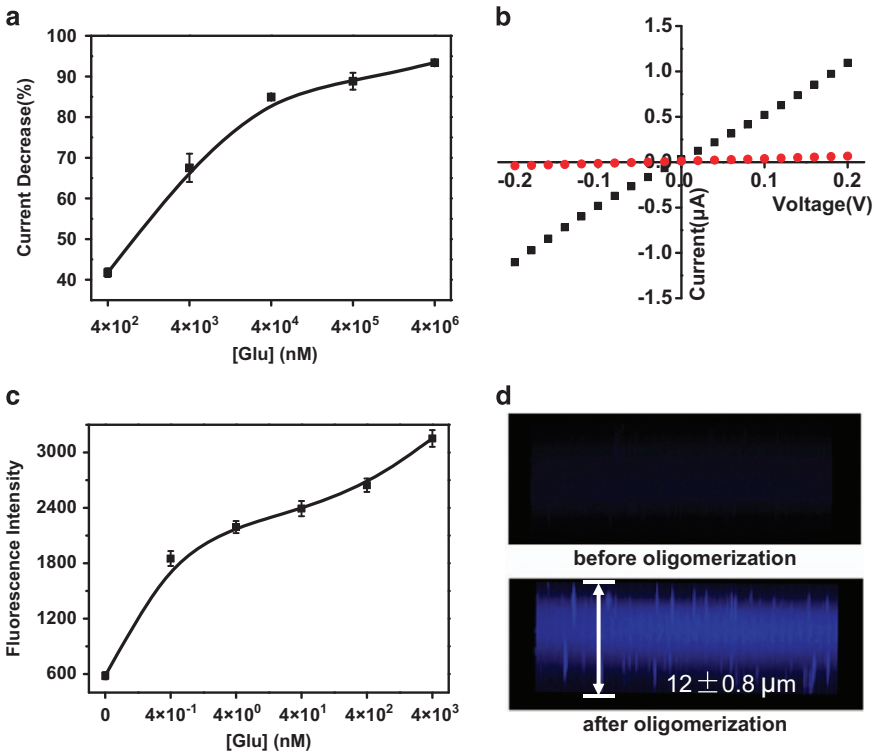

Figure 4 Detection of glucose (Glu), as monitored by nanochannel conductance. (**a**) Current change ratios measured at 0.2 V in the presence of different concentrations of Glu. (**b**) Current-voltage (I-V) curve for the nanochannels before (black square) and after (red circle) embedding in Glu and ((1,2-diphenylethene-1,2-diyl) bis (1,4-phenylene)-1,1′-diboronic acid (TPEDB)). Fluorescence response to Glu, characterized by laser scanning confocal microscope (LSCM). (**c**) Fluorescence intensity of modified nanochannels in response to different concentrations of Glu. (**d**) LSCM observation of the nanochannels membrane before (top) and after (bottom) Glu (4 μM) and TPEDB (50 μM) oligomerization. The membrane thickness is ~12 μM.

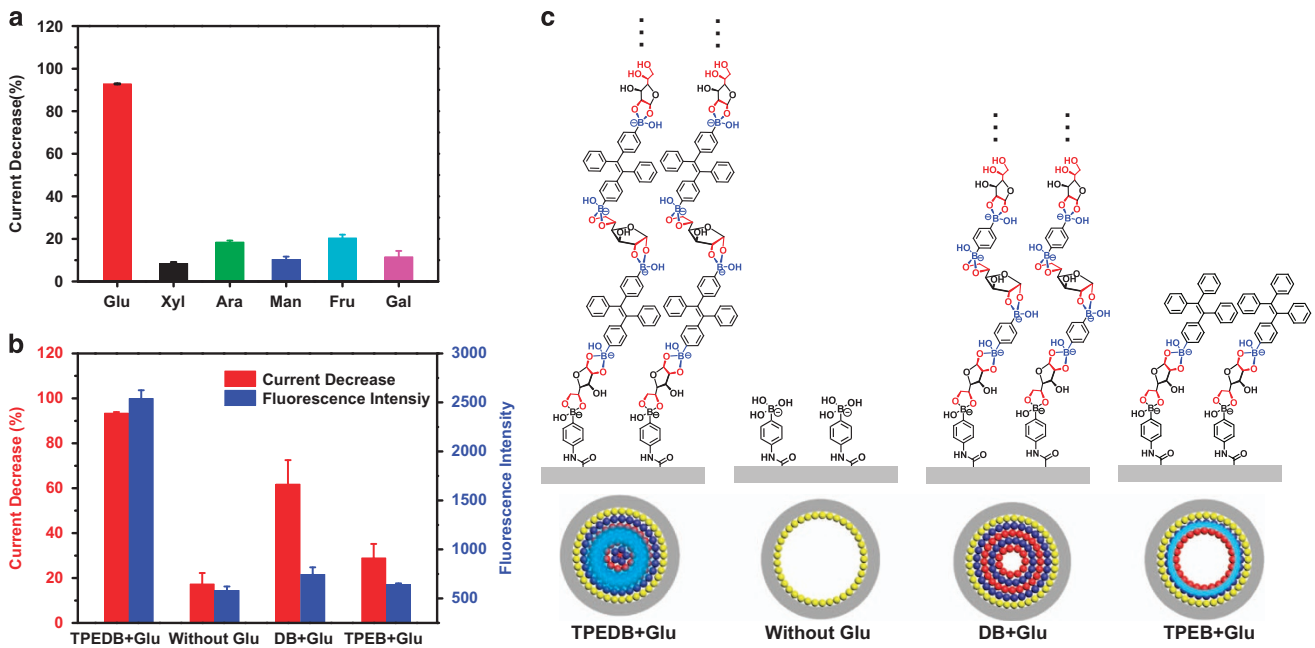

Figure 5 (**a**) Dual-signal-output nanochannels show a good specificity for glucose. Compared with glucose, the signal decrease of other monosaccharides is much lower. (**b**) Current change ratio and fluorescence intensity of dual-signal-output system for (4-(1,2,2-triphenylvinyl)phenylboronic acid (TPEB) and 1,4-benzenediboronic acid (DB). (**c**) Proposed mechanism and the chemical structure of the systems, ((1,2-diphenylethene-1,2-diyl) bis (1,4-phenylene)-1,1′-diboronic acid (TPEDB))+Glu, without Glu, TPEB+Glu and DB+Glu, on the walls of the nanochannels.

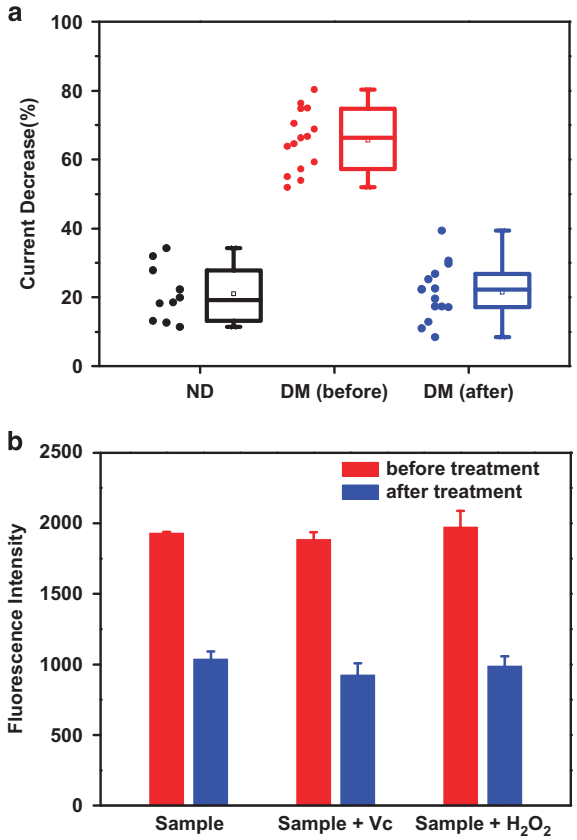

Figure 6 (**a**) Results of the applicability of the system in diabetes diagnosis. Signal decrease of this system in response to 40 urine samples (10 normal individuals' urine samples (ND) and the urine samples of 15 diabetes patients (DM) before and after treatment). All of the urine specimens were obtained from the Union Hospital of Tongji Medical College (Wuhan, Hubei, China). (**b**) Fluorescence intensity of dual-signal-output nanochannels in urine samples (DM10) spiked with Vc or H_2O_2. Error bars indicate the s. d. of triplicate tests.

obvious change (Figure 5b). Moreover, another chemical, 1,4-benzenediboronic acid (DB, Supplementary Figure S11), that possesses two boronic acid units but cannot emit light is chosen for examination in this system. Understandably, a >60% ionic current decrease and little change in fluorescence are observed in the Glu solution (Figures 5b and c). The striking contrast among the experimental data from the systems, TPEDB+Glu, TPEDB, DB+Glu and TPEB+Glu, offers strong support for the proposed mechanism shown in Figure 1.

Glu monitoring for diabetes is usually performed on blood or urine samples; the latter samples are collected in a noninvasive manner and can provide very valuable information about related diseases. Therefore, the urine Glu level is an important clinical indicator for the screening and monitoring of diabetes. To verify our proposed theory in this study and to evaluate the applicability in diabetes diagnosis, 40 urine specimens from diabetes patients (DM) before and after treatment (insulin injection or other drug therapy) and normal individuals (ND) are investigated (Figure 6a, Supplementary Figures S12 and S13 and Supplementary Table S1). As shown in Figure 6a, the signals from diabetes patients after treatment return to the normal level and are lower than that before treatment. The discrimination ability of our PBA-modified nanochannels is also investigated by laser scanning confocal microscopy (Supplementary Figure S14). All these results are consistent with the clinical diagnoses, indicating the reliability of the tests. Because urine-glucose detection using glucose oxidase is based on redox reactions, reducing or oxidizing compounds may interfere with the testing procedures and lead to false results. In our method, the dual-signal-output nanochannels do not rely on the redox reaction. Thus, our method can effectively avoid the interference caused by ascorbic acid (Vc) and H_2O_2; this ability reflects another attractive advantage of this system in practical applications (Figure 6b and Supplementary Figure S15).

CONCLUSIONS

In conclusion, utilizing dual-signal-output nanochannels that involve the combination of ionic current with fluorescence, we presented direct evidence that current-blockade events correspond to the gating process of nanochannels. Furthermore, the implementation of both ionic current and fluorescence analysis of nanochannels can easily reveal that the gatekeepers (here, oligomers) open and close the nanochannels via an onion-like intermediate state, which is also consistent with the MD simulations. Taking advantage of the oligomerization reaction between the AIE molecule (TPEDB) and Glu, we can simultaneously observe ionic current reduction and fluorescence enhancement in the presence of Glu; this approach shows a high sensitivity and selectivity for Glu. To examine the clinical test capabilities of this approach, 40 urine specimens (10 normal individuals' urine samples and the urine samples of 15 diabetes patients before and after treatment) were investigated. All of the results were consistent with those given by standard assays used in hospitals, indicating the reliability of our method. Moreover, these dual-signal-output nanochannels showed a high antijamming property with regard to impurities such as Vc and H_2O_2 in complicated practical environments. The utilization of AIE molecule-based oligomerization thus offers a new strategy for the development of a smart gate, from single–to-dual signals, and would promote the application of smart nanochannels in complex environments for diagnostics, drug metabolism monitoring and biomolecule transport processes.

CONFLICT OF INTEREST

The authors declare no conflict of interest.

ACKNOWLEDGEMENTS

This work is supported by the National Basic Research Program of China (973 program, 2015CB932600 and 2013CB933000), the National Natural Science Foundation of China (21574048, 21375042, 21574048, 21405054, and 51273053), the Natural Science Foundation of Hubei Province of China (2014CFB1012).

1 Ashcroft, F. M., Harrison, D. E. & Ashcroft, S. J. Glucose induces closure of single potassium channels in isolated rat pancreatic β-cells. *Nature* **312**, 446–448 (1984).
2 Kim, B. E., Nevitt, T. & Thiele, D. J. Mechanisms for copper acquisition, distribution and regulation. *Nat. Chem. Biol.* **4**, 176–185 (2008).
3 Martin, C. R. & Siwy, Z. S. Learning nature's way: biosensing with synthetic nanopores. *Science* **317**, 331–332 (2007).
4 Ali, M., Yameen, B., Neumann, R., Ensinger, W., Knoll, W. & Azzaroni, O. Biosensing and supramolecular bioconjugation in single conical polymer nanochannels. facile incorporation of biorecognition elements into nanoconfined geometries. *J. Am. Chem. Soc.* **130**, 16351–16357 (2008).
5 Ali, M., Nasir, S., Nguyue, Q. H., Sahoo, J. K., Tahir, M. N., Tremel, W. & Ensinger, W. Metal ion affinity-based biomolecular recognition and conjugation inside synthetic polymer nanopores modified with iron–terpyridine complexes. *J. Am. Chem. Soc.* **133**, 17307–17314 (2011).
6 Wang, M., Sun, C., Wang, L., Ji, X., Bai, Y., Li, T. & Li, J. H. Electrochemical detection of DNA immobilized on gold colloid particles modified self-assembled monolayer electrode with silver nanoparticle label. *J. Pharm. Biomed. Anal.* **33**, 1117–1125 (2003).

7 Duan, R., Zuo, X., Wang, S., Quan, X., Chen, D., Chen, Z., Jiang, L., Fan, C. & Xia, F. Quadratic isothermal amplification for the detection of microRNA. *Nat. Protoc.* **9**, 597–607 (2014).
8 Gao, A., Lu, N., Wang, Y., Dai, P., Li, T., Gao, X., Wang, Y. & Fan, C. Enhanced sensing of nucleic acids with silicon nanowire field effect transistor biosensors. *Nano Lett.* **12**, 5262–5268 (2012).
9 Lin, M., Wang, J., Zhou, G., Wang, J., Wu, N., Lu, J., Gao, J., Chen, X., Shi, J., Zuo, X. & Fan, C. Programmable engineering of a biosensing interface with tetrahedral DNA nanostructures for ultrasensitive DNA detection. *Angew. Chem. Int. Ed.* **54**, 2151–2155 (2015).
10 Ying, Y., Zhang, J., Gao, R. & Long, Y. Nanopore-based sequencing and detection of nucleic acids. *Angew. Chem. Int. Ed.* **52**, 13154–13161 (2013).
11 Daiguji, H. Ion transport in nanofluidic channels. *Chem. Soc. Rev.* **39**, 901–911 (2010).
12 Zhang, F., Nangreave, J., Liu, Y. & Yan, H. Structural DNA nanotechnology: state of the art and future perspective. *J. Am. Chem. Soc.* **136**, 11198–11211 (2014).
13 Wang, G., Bohaty, A. K., Zharov, L. & White, H. S. Photon gated transport at the glass nanopore electrode. *J. Am. Chem. Soc.* **128**, 13553–13558 (2006).
14 Kalman, E. B., Vlassiouk, I. & Siwy, Z. S. Nanofluidic bipolar transistors. *Adv. Mater.* **20**, 293–297 (2008).
15 Vlassiouk, I., Apel, P. Y., Dmitriev, S. N., Healy, K. & Siwy, Z. S. Versatile ultrathin nanoporous silicon nitride membranes. *Proc. Natl Acad. Sci. USA* **106**, 21039–21044 (2009).
16 Baker, L. A. & Bird, S. P. Nanopores: a makeover for membranes. *Nat. Nanotechnol.* **3**, 73–74 (2008).
17 Van den Hout, M., Kruddle, V., Janssen, X. J. A. & Dekker, N. H. Distinguishable populations report on the interactions of single DNA molecules with solid-state nanopores. *Biophys. J.* **99**, 3840–3848 (2010).
18 Vlassarev, D. M. & Golovchenko, J. Trapping DNA near a solid-state nanopore. *Biophys. J.* **103**, 352–356 (2012).
19 Buchsbaum, S. F., Nguyen, G., Howorka, S. & Siwy, Z. S. DNA-modified polymer pores allow pH- and voltage-gated control of channel flux. *J. Am. Chem. Soc.* **136**, 9902–9905 (2014).
20 Aksimentiev, A., Heng, J. B., Timp, G. & Schulten, K. Microscopic kinetics of DNA translocation through synthetic nanopores. *Biophys. J.* **87**, 2086–2097 (2004).
21 Ando, G., Hyun, C., Li, J. & Mitsui, T. Directly observing the motion of DNA molecules near solid-state nanopores. *ACS Nano* **6**, 10090–10097 (2012).
22 Menard, L. W., Mair, C. E., Woodson, M. E., Alarie, J. P. & Ramsey, J. M. A device for performing lateral conductance measurements on individual double-stranded DNA molecules. *ACS Nano* **6**, 9087–9094 (2012).
23 Soni, G. V., Singer, A., Yu, Z., Sun, Y., McNally, B. & Meller, A. Synchronous optical and electrical detection of biomolecules traversing through solid-state nanopores. *Rev. Sci. Instrum.* **81**, 014301 (2010).
24 Heron, A. J., Thompson, J. R., Cronin, B., Bayley, H., Mark, I. & Wallace, M. I. Simultaneous measurement of ionic current and fluorescence from single protein pores. *J. Am. Chem. Soc.* **131**, 1652–1653 (2009).
25 Liu, S., Zhao, Y., Parks, J. W., Deamer, D. W., Hawkins, A. R. & Schmidt, H. Correlated electrical and optical analysis of single nanoparticles and biomolecules on a nanopore-gated optofluidic chip. *Nano Lett.* **14**, 4816–4820 (2014).
26 Ivankin, A., Henley, R. Y., Larkin, J., Carson, S., Toscano, M. L. & Wanunu, M. Label-free optical detection of biomolecular translocation through nanopore arrays. *ACS Nano* **8**, 10774–10781 (2014).
27 Li, Y., Zheng, Y. & Zare, R. N. Electrical, optical, and docking properties of conical nanopores. *ACS Nano* **6**, 993–997 (2012).
28 Kurz, V., Nelson, E. M., Shim, J. & Timp, G. Direct visualization of single-molecule translocations through synthetic nanopores comparable in size to a molecule. *ACS Nano* **7**, 4057–4069 (2013).
29 McNally, B., Singer, A., Yu, Z., Sun, Y., Weng, Z. & Meller, A. Optical recognition of converted DNA nucleotides for single-molecule DNA sequencing using nanopore arrays. *Nano Lett.* **10**, 2237–2244 (2010).
30 Schibel, A. E. P., Heider, E. C., Harris, J. M. & White, H. S. Fluorescence microscopy of the pressure-dependent structure of lipid bilayers suspended across conical nanopores. *J. Am. Chem. Soc.* **133**, 7810–7815 (2011).
31 Lou, X., Zhao, Z., Hong, Y., Dong, C., Min, X., Zhuang, Y., Xu, X., Jia, Y., Xia, F. & Tang, B. Z. A new turn-on chemosensor for bio-thiols based on the nanoaggregates of a tetraphenylethene-coumarin fluorophore. *Nanoscale* **6**, 14691–14696 (2014).
32 Liu, Y., Deng, C., Tang, L., Qin, A., Hu, R., Sun, J. & Tang, B. Z. Specific detection of d-glucose by a tetraphenylethene-based fluorescent sensor. *J. Am. Chem. Soc.* **133**, 660–663 (2011).
33 Lou, X., Zhuang, Y., Zuo, X., Jia, Y., Hong, Y., Min, X., Zhang, Z., Xu, X., Liu, N., Xia, F. & Tang, B. Z. Real-Time, quantitative lighting-up detection of telomerase in urines of bladder cancer patients by AIEgens. *Anal. Chem.* **87**, 6822–6827 (2015).
34 Xia, F., Guo, W., Mao, Y., Hou, X., Xue, J., Xia, H., Wang, L., Song, Y., Ji, H., Ouyang, Q., Wang, Y. & Jiang, L. Gating of single synthetic nanopores by proton-driven DNA molecular motors. *J. Am. Chem. Soc.* **130**, 8345–8350 (2008).
35 Liu, N., Jiang, Y., Zhou, Y., Xia, F., Guo, W. & Jiang, L. Two-way nanopore sensing of sequence-specific oligonucleotides and small-molecule targets in complex matrices using integrated DNA supersandwich structures. *Angew. Chem. Int. Ed.* **52**, 2007–2011 (2013).
36 Guo, W., Hong, F., Liu, N., Huang, J., Wang, B., Duan, R., Lou, X. & Xia, F. Target-specific 3D DNA gatekeepers for biomimetic nanopores. *Adv. Mater.* **27**, 2090–2095 (2015).
37 Cornell, W. D., Cieplak, P., Bayly, C. I., Gould, I. R., Merz, K. M., Ferguson, D. M., Spellmeyer, D. C., Fox, T., Caldwell, J. W. & Kollman, P. A. A second generation force field for the simulation of proteins, nucleic acids, and organic molecules. *J. Am. Chem. Soc.* **117**, 5179–5197 (1995).
38 Zhang, M., Qing, G., Xiong, C., Cui, R., Pang, D. & Sun, T. Dual-responsive gold nanoparticles for colorimetric recognition and testing of carbohydrates with a dispersion-dominated chromogenic process. *Adv. Mater.* **25**, 749–754 (2013).
39 Lee, J. W., Lee, J. S. & Chang, Y. T. Colorimetric identification of carbohydrates by a pH indicator/pH change inducer ensemble. *Angew. Chem. Int. Ed.* **45**, 6485–6487 (2006).
40 Norrild, J. C. & Eggert, H. Evidence for mono-and bisdentate boronate complexes of glucose in the furanose form. application of 1JC-C coupling constants as a structural probe. *J. Am. Chem. Soc.* **117**, 1479–1484 (1995).

Supplementary Information accompanies the paper on the NPG Asia Materials website (http://www.nature.com/am)